Journal of Power Sources 195 (2010) 3893–3899

Contents lists available at ScienceDirect

Journal of Power Sources

journal homepage: www.elsevier.com/locate/jpowsour

Enhanced lithium-ion intercalation properties of coherent hydrous vanadium pentoxide–carbon cryogel nanocomposites

Anqiang Pan[a,b], Dawei Liu[a], Xiaoyuan Zhou[a], Betzaita Betalla. Garcia[a], Shuquan Liang[b], Jun Liu[c], Guozhong Cao[a,*]

[a] Department of Materials Science and Engineering, University of Washington in Seattle, 302 Roberts Hall, Box 352120, Seattle, WA 352120, USA
[b] Department of Materials Science and Engineering, Central South University, Hunan 410083, People's Republic of China
[c] Pacific Northwest National Laboratory Richland, Washington 99352, USA

ARTICLE INFO

Article history:
Received 22 November 2009
Received in revised form
23 December 2009
Accepted 29 December 2009
Available online 14 January 2010

Keywords:
Hydrous vanadium pentoxide
Carbon cryogels
Potentiodynamic deposition
Coherent nanocomposite
Discharge capacity

ABSTRACT

Coherent hydrous vanadium pentoxide ($V_2O_5 \cdot nH_2O$)–carbon cryogel (CC) nanocomposites were synthesized by electrodeposition of vanadium pentoxide onto the porous carbon scaffold which was derived from resorcinol (R) and formaldehyde (F) organic hydrogels. As-fabricated nanocomposites were characterized by scanning electron microscopy (SEM), along with EDAX and nitrogen sorption isotherms which suggested vanadium pentoxide incorporated in the pores of carbon cryogels. The nanocomposites showed much improved discharge capacity and better cyclic stability as compared to hydrous vanadium pentoxide films deposited on platinum foil. The discharge capacity of the nanocomposites reached 280 mAh g^{-1} based on the mass of the vandium pentoxide at a current density of 100 mA g^{-1} and it possessed good cycle stability at different discharge rates. The results demonstrated that electrochemical performances, such as specific discharge capacitance and reversibility of the composite electrode, could be greatly enhanced by the introduction of carbon cryogels (CCs) scaffold with three-dimensionally interconnected porous structure in which $V_2O_5 \cdot nH_2O$ homogeneously dispersed.

1. Introduction

Lithium-ion batteries have replaced much of older battery systems like nickel metal hydride, and particularly have been used for today's high-tech devices, such as laptops and cell phones mainly due to their high energy density and long cycle life [1,2]. Recently, with the increasing awareness and demands for clean and sustainable energy, lithium-ion batteries are also entering the plug-in hybrid electric-vehicle market and are a serious contender to power the electric cars of the future [3]. However, lithium-ion batteries still cannot satisfy the needs for high specific power and energy storage applications such as power tools, electric vehicles or efficient use of renewable energies [4]. Developing new cathode and anode materials with better energy storage properties has become an urgent demand to meet the increasing requirements to the new technologies and industries.

Vanadium pentoxide has been one of the attractive candidate cathode materials for a long time largely, due to its high energy density, intercalation voltage (vs. the anode material), reversibility, and stability [5–7]. Electrochemical lithium-ion insertion occurs together with compensating electrons as follows [8,9]:

$$xLi^+ + xe^- + V_2O_5 \rightarrow Li_xV_2O_5 \quad (1)$$

However, the intrinsic low diffusion coefficient of lithium ions in crystalline V_2O_5, i.e., $D \sim 10^{-12}$ cm^2 s^{-1} [10] hinders the practical wide-spread utilization of this material as cathode in lithium-ion batteries. For efficient lithium-ion intercalation, it is necessary to have coordinated and efficient mass and charge transport through the solid electrodes and redox reactions at the interface between the electrodes and the liquid electrolyte. Nanostructured vanadium pentoxide, such as in the form of nanorod, nanotube, and nanocable arrays, has demonstrated much improved lithium-ion intercalation properties due to reduced diffusion distance for both lithium ions and electrons and much increased surface area for intercalation–deintercalation reactions so that the specific power can be improved; nanostructured electrodes with huge surface area, thus large surface energy, also facilitate the phase transition leading to much enhanced reversible storage capacity [7,11–13]. It has been reported that vanadium pentoxide aerogels and xerogels as electroactive materials when used as cathode in lithium-ion batteries reached a high capacity, up to 400 mAh g^{-1} [13,14].

The low electronic conductivity of V_2O_5 is another key factor that should be addressed for applications as an electrode material. Composites of V_2O_5 with highly electrical conductive materials,

* Corresponding author. Fax: +1 206 543 3100.
E-mail address: gzcao@u.washington.edu (G. Cao).

0378-7753/$ – see front matter © 2010 Elsevier B.V. All rights reserved.
doi:10.1016/j.jpowsour.2009.12.120

such as conductive polymer [15,16] metal fibers [12] or carbonaceous materials, have attracted great attention for lithium-ion batteries. Among these materials, carbonaceous materials are the most attractive because of its good conductivity, flexibility and low density. Composites of vanadium pentoxide or hydrous V_2O_5 mixed with carbon nanotubes (CNTs) have been fabricated and studied; such composite possessed good lithium-ion intercalation properties [17,18]. Recently, carbon tube-in-tube materials (CTITs) which built by a narrower inner tube inside an outer tube in combination with nanosized V_2O_5 owned good lithium permeation and electrochemical stability [19]. Such nanocomposites provide favorable diffusion pathways for both electrons and lithium-ions, which are essential for high-rate rechargeable lithium-ion batteries.

Carbon cryogels, derived from organic hydrogels, first made via polycondensation of resorcinol (R) and formaldehyde (F) under slightly basic aqueous conditions by Pekala [20] have been widely explored for supercapacitor applications. Typically the key factors in determining the morphology of the final product are the ratios of R/F and R/C (catalyst), as well as the concentration of the reactants in the aqueous solution (R/W). After drying these hydrogels with supercritical fluids or freeze-drying, pyrolysis at high temperature can produce widely researched carbon aerogels [21–24] and more cost-efficient carbon cryogels, respectively. As-fabricated sol-gel derived carbon nanoarchitectures are particularly attractive for electrochemical capacitor applications due to their inherent structural characteristics that include high specific surface areas, through-connected networks of mesopores and micropores, tunable pore sizes ranging from nanometers to micrometers, durable monolithic, moldable forms and good electronic conductivity (10–40 S cm^{-1}) [25,26]. Carbon cryogels, due to these attractive properties, have been shown to be used to good effects as supercapacitors [27,28] as well as scaffolds for chemical species to be utilized, for example, in hydrogen storage materials [29,30].

Electrochemical deposition is a facile and cost effective way to fabricate metal oxide and it has been empolyed to make hydrous vanadium pentoxide thin film on substrate by anodic electrodeposite from $VOSO_4$ solution under particular conditions [31]. Template-based nanorods and nanotubes arrays [32,33] were successfully fabricated by electrodeposition hydrous vanadium pentoxide into polycarbonate template in our early reports, which suggested high initial capacity, which demonstrated higher discharge capacity and better cycle stability. In this research work, we report nanoscale hydrous vanadium pentoxide deposits can be achieved throughout the mesoporous carbon cryogels using potentiodynamic electrodeposition. As-synthesized nanocomposites exhibited high initial discharge capacitance of 280 mAh g^{-1} and remained 257 mAh g^{-1} after 20 cycles charge/discharge based on the total mass of the nanocomposites at a current density of 100 mA g^{-1}.

2. Experimental

2.1. Carbon cryogels fabrication

Resorcinol–formaldehyde (RF) derived carbon cryogels (CCs) were prepared with a procedure similar to the literature previously reported. The recipe is briefly shown as follows: resorcinol (99+%, Sigma–Aldrich, USA) and formaldehyde (37% solution, J.T. Baker, USA) dissolved in distilled water (W), using sodium carbonate (99.5%, Sigma–Aldrich, USA) as a catalyst (C). The R/W ratio was 0.035 g ml^{-1}. Molar ration of R/C and R/F ratio were 200:1and 1:2 respectively. The solutions were sealed and cured at 90 °C for 7 days to complete the gelation process. After solvent exchange, all the samples were freeze-dried for a week under vacuum (at −50 °C) to obtain the RF hydrogels and then pyrolyzed in nitrogen at 1050 °C for 4 h to produce carbon cryogels (CCs). After pyrolysis, the CCs were mixed with polytetrafluoroethylene (PTFE, 3 wt%) and pressed to produce the electrode discs, the thickness of which was about 50 μm.

2.2. Synthesis of coherent $V_2O_5{\cdot}nH_2O$–CC nanocomposites

CCs film was fixed between two platinum meshes and held tightly by a PTFE framed grid sample holder and then was immersed in the $VOSO_4$ solution (pH 1.8) in a sub-atmospheric pressure chamber (about 225 mm of Hg) for 1 h to ensure complete infusion of the $VOSO_4$ solution into pores of the CCs film. The potentiodynamic electrodeposition was carried out at a voltage ranging from 0.6 to 2.0 V vs. Ag/AgCl at a scan rate of 50 mV s^{-1} for up to 300 cycles using CHI605B potentiostat/galvaostat (CHI. Inc., USA) instrument. Platinum foil was used as the counter electrode. After 300 cycles of potentiodynamic deposition, the carbon cryogel films were removed from the electrochemical deposition beaker, and soaked and rinsed in DI water. Then the film was dried at room temperature in ambient for 24 h. For comparison, hydrous V_2O_5 thin films were prepared by the same method onto platinum foil substrates under the same conditions. The film samples were dried under vacuum at 80 °C overnight and weighed prior to and after the potentiodynamic electrodeposition with a XS205 DualRange (Mettler Toledo, Columbus, OH). The weight density for hydrous vanadium pentoxide on Pt foil and coherent hydrous V_2O_5–CCs nanocomposites were 0.6 and 0.4 mg cm^{-2} respectively.

2.3. SEM, EDXS, XRD and nitrogen sorption isotherms

The morphologies of the coherent hydrous V_2O_5–CC nanocomposites were analyzed by means of scanning electron microscopy (SEM, JEOL JSM 7000F) and elemental compositional analysis of the cross-section by means of energy dispersive X-ray spectroscopy (EDS, JSM 7000, Philips JEOL, Peabody, MA). X-ray diffraction (XRD) using a Philips PW1820 diffractometer with Cu Ka radiation was employed to determine the crystal structure and grain size of crystalline phase after vacuum drying at 80 °C and after annealing in air at 400 °C for 2 h. Nitrogen sorption isotherms using a Quantachrome NOVA 4200e instrument was carried out to detect the porous structure of both CCs and nanocomposites. Specific surface area, pore volume and pore sizes were calculated using multi-point BET, *t*-method, and BJH methods respectively.

2.4. Electrochemical analysis of coherent $V_2O_5{\cdot}nH_2O$–CC nanocomposites

The charge/discharge measurements were carried out at different current densities based on the mass of vanadium pentoxide employing Chronopotentiometric technique and cyclic voltammetry (CV) curves were obtained by cyclic voltammetry technique. Both measurements were performed using potentiaostat/galvanostat (CHI605B, USA) workshop with Ag/$AgNO_3$ (0.001 M $AgNO_3$ in propylene carbonate) as reference electrode and platinum foil as the counter electrode. The operating voltage was controlled between 0.5 and −1.5 V vs. the Ag/Ag^+ and the electrolyte was 1 M $LiClO_4$ dissolving in propylene carbonate (PC).

3. Results and discussion

Although no difference between the samples before and after hydrous vanadium oxide deposition was observed by naked eyes, SEM observation revealed a noticeable change of the brightness of film samples from original total “black” (easy electron dissipation) of carbon cryogel film to “gray” (electrostatic charge as electrons accumulated) of the film with hydrous vanadium oxide deposition

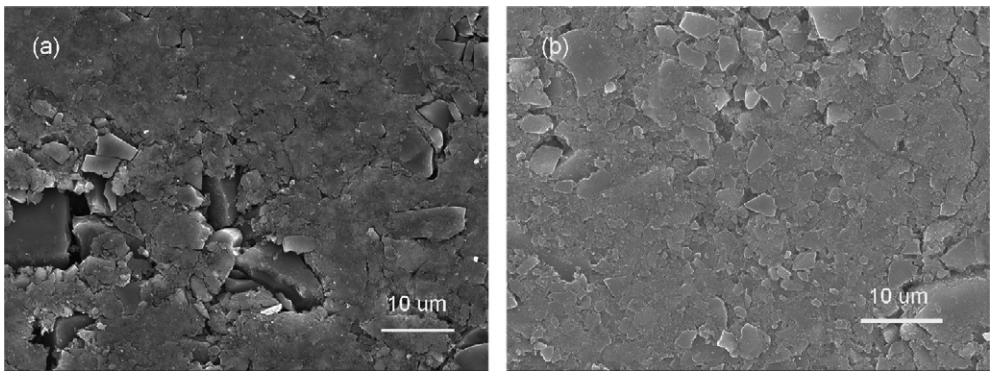

Fig. 1. SEM patterns for carbon cryogel before deposition (a) and after deposition (b).

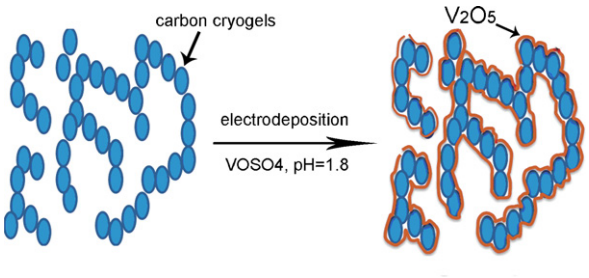

Scheme 1. Schematical illustrating the synthesis and microstructure of coherent nanocomposites in which hydrous V_2O_5 deposited and coated onto surface carbon cryogel scaffold.

(Fig. 1). This was attributed to the fact that the deposition or coating of hydrous vanadium pentoxide to the carbon cryogel films resulted in a reduction of electrical conductivity, as hydrous vanadium pentoxide possesses a much lower electrical conductivity than that of carbon network. A 33% weight increase was detected, equivalent to the weight ratio of $V_2O_5{\cdot}nH_2O$:CCs = 25:75 according to the mass change of carbon cryogel film although there is no detectable change in the dimensions of the carbon cryogel film. The increase of the weight indicated the successful loading of extra materials to the films.

Fig. 1 shows the scheme of synthesis of nanocomposites by electrodeposition of hydrous vanadium pentoxide inside the pores of carbon cryogel films and the reactions occurs as follows:

$$2VO^{2+} + 3H_2O \rightarrow V_2O_5 + 6H^+ + 2e \quad (2)$$

This reaction can be readily realized in aqueous solution at pH 1.8 through oxidation of V^{4+} to V^{5+} according to the literature [31]. The formation of hydrous vanadium pentoxide can be proved by the rapid increase of oxidation current density starting from 1.1 V and reached a maximum at 1.5 V (vs. Ag/AgCl) (shown in Fig. 2). With the increased number of sweeping cycles, the current density of oxidation peaks continuously became lower due to the formation of relatively insulating hydrous vanadium pentoxide coating on the surface of carbon scanffold. At potentials higher than 1.7 V, second rapid increase of current density was observed which is corresponding to the oxidation of water.

The surface morphologies of as-fabricated hydrous vanadium pentoxide–carbon cryogel nanocomposites were shown in Fig. 3a. It demonstrated a homogeneous morphology across the sample, suggesting uniform deposition of hydrous vanadium pentoxide throughout the porous carbon cryogel film, in contrast to a coated layer of oxide on the exterior surface of carbon cryogel film. EDAX analyses were carried out on both the surface and cross-section of the nanocomposites. The detection of vanadium element peaks of the cross-section (i.e., inside the film) again suggesting the deposition of hydrous vanadium pentoxide throughout the entire porous structure of carbon cryogel film, although the intensity of vanadium element peak at the surface of the nanocomposite film is a little stronger than that inside the film. The element mapping on the cross-section of nanocomposite film was shown in Fig. 4, which further indicates the homogeneous distribution of vanadium element (corresponding to V_2O_5) throughout the entire sample.

Fig. 5 shows the nitrogen sorption isotherms for both coherent $V_2O_5{\cdot}nH_2O$–CC nanocomposites and pristine carbon scanffold samples which exhibit typical IV isotherm [34], with the hysteresis associated with the dominance of mesoporosity. After deposition of hydrous vanadium pentoxide, the amount of nitrogen adsorbed to the sample decreased significantly (Fig. 5a), which suggested a decrease in pore volume in coherent nanocomposites as compared to pristine carbon cryogels. The pore size distribution of carbon cryogels and coherent carbon cryogel–hydrous vanadium pentoxide nanocmposites (Fig. 5b) shows the peak pore size shifted to a smaller size after the deposition of hydrous vanadium pentoxide. The highly mesoporous structure of the two samples were detailed in Table 1. After the electrodeposition of hydrous vanadium oxide, the pore volume reduced significantly from the original 0.98–0.42 cc g^{-1}, with more than 50% reduction and the peak pore size decreased from 8 to 6 nm in diameter and the surface area decreased to 402 from 572 $m^2\,g^{-1}$. The reduction in the pore volume, pore size and specific surface area were all presumably due to the successfully deposition of hydrous vanadium pentoxide inside

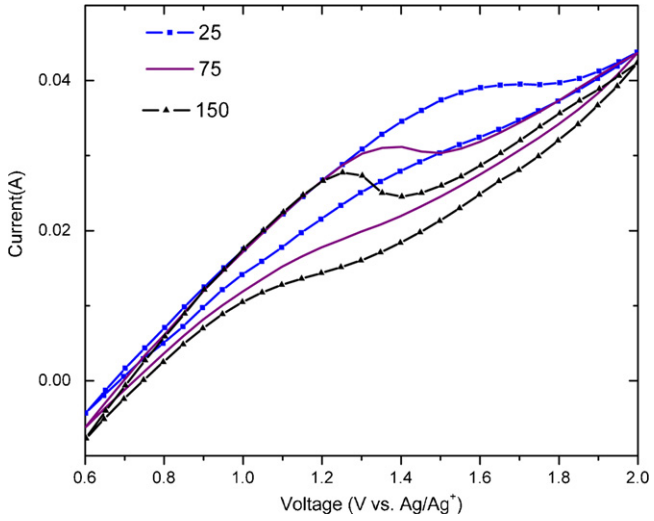

Fig. 2. Cyclic voltammetry curves for deposition on carbon cryogels in the voltage range of 0.6–2.0 V vs. Ag/Ag^+ at a scan rate of 50 mV s^{-1} with the solution of 0.1 M $VOSO_4$. The pH was adjusted to 1.8.

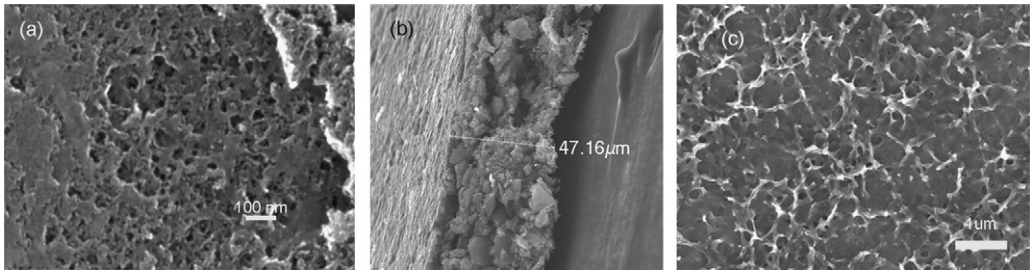

Fig. 3. Scanning electron microscope (SEM) images of $V_2O_5{\cdot}nH_2O$–CC nanocomposites surface morphology (a), cross-section (b) and surface morphology of $V_2O_5{\cdot}nH_2O$ thin film on Pt substrate (c).

Table 1
Nitrogen adsorption analyses data of pristine CC and $V_2O_5{\cdot}nH_2O$–CCs nanocomposite.

Samples	Carbon cryogels(CCs)	$V_2O_5{\cdot}nH_2O$–CCs
S_{BET} ($m^2\,g^{-1}$)	570	402
Mesoporous volume ($cc\,g^{-1}$)	0.98	0.42
Pore size (nm)	8	6

the pores of carbon cryogel, which took some of the void space and thus resulted in the change of the porous structure.

The XRD patterns of the coherent carbon cryogels–hydrous vanadium pentoxide nanocomposites before (a) and after thermal annealing (b) are shown in Fig. 6. No characteristic peaks were detected for nanocomposites before thermal annealing, which indicated the amorphous nature of the nanocomposites. When annealed at 400 °C in air for 2 h, it changed into crystallized V_2O_5, as indicated by XRD pattern of orthorhombic V_2O_5 (JCPDS card No. 41-1426).

Fig. 7 displays the cyclic voltammograms of the $V_2O_5{\cdot}nH_2O$–CCs nanocomposite, $V_2O_5{\cdot}nH_2O$ film, and pristine CCs film electrodes, measured using the electrolyte consisting of 1 M $LiClO_4$ in PC at the potential scan rate of $1\,mV\,s^{-1}$. The voltage window was set between −1.5 and 0.5 V (vs. $Ag/AgNO_3$) and the current density was normalized to the mass of the samples. Two current peaks at around −0.85 and −0.6 V vs. Ag/Ag^+ in the anodic scan and two peaks at around −1.0 and −0.7 V vs. Ag/Ag^+ in the cathodic scan were identified in the CV curves of the V_2O_5 thin film. It is believed

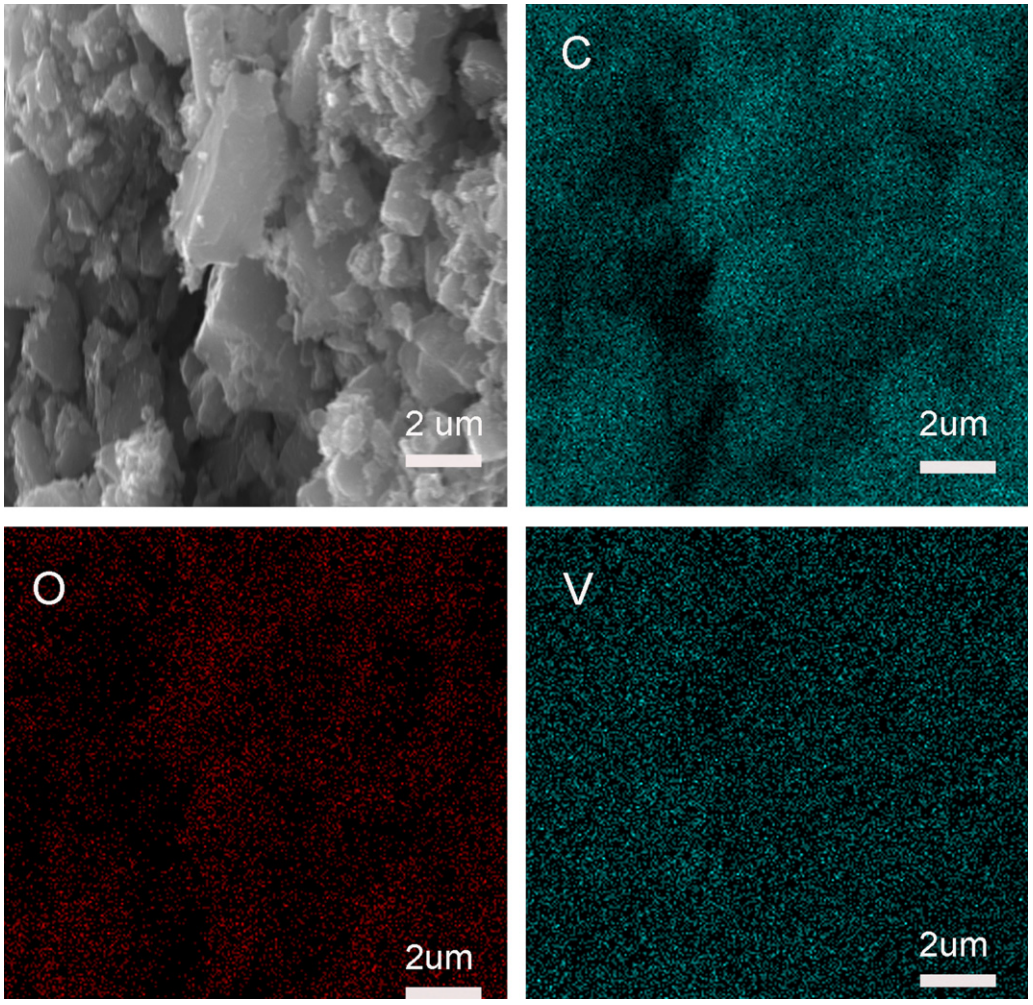

Fig. 4. SEM image (top left) and elemental mapping (carbon: top right, oxygen: bottom left, and vanadium: bottom right) of the cross-section of the nanocomposites.

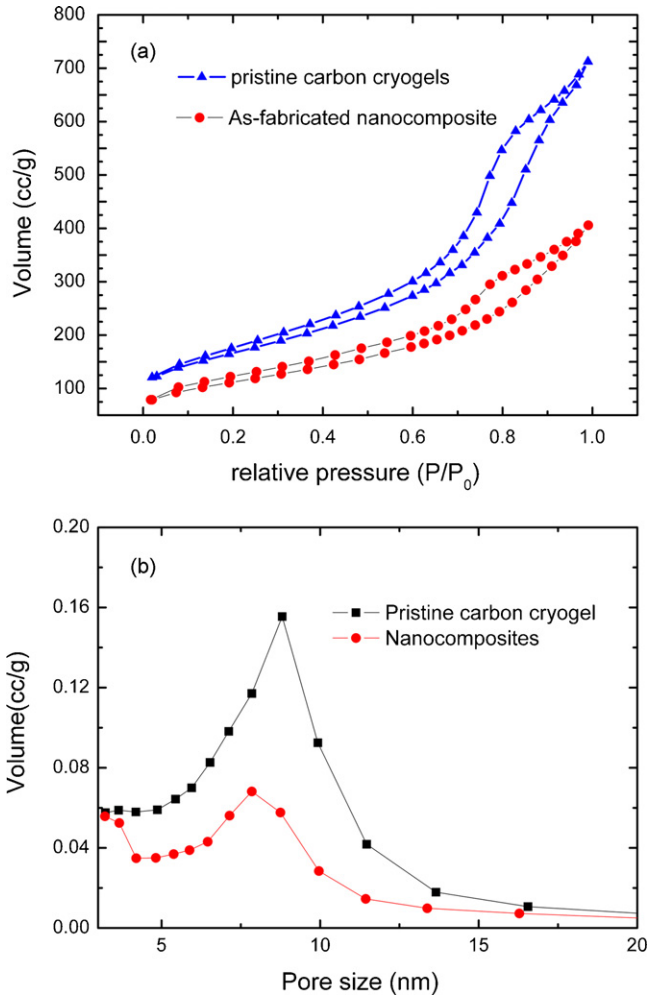

Fig. 5. Nitrogen sorption isotherms (a) and pore size distribution (b) for $V_2O_5{\cdot}nH_2O$–CC nanocomposites and pristine CCs.

that the pairs of anodic and cathodic peaks in the CV curve are related to the Li-ion intercalation and deintercalation, respectively [35]. For the coherent hydrous vanadium pentoxide–carbon cryogel nanocomposites, peaks were broader and overlapped centered near −0.7 V in the cathodic scan and −0.6 V in the anodic scan. These changes may be attributed to the different electrochemical

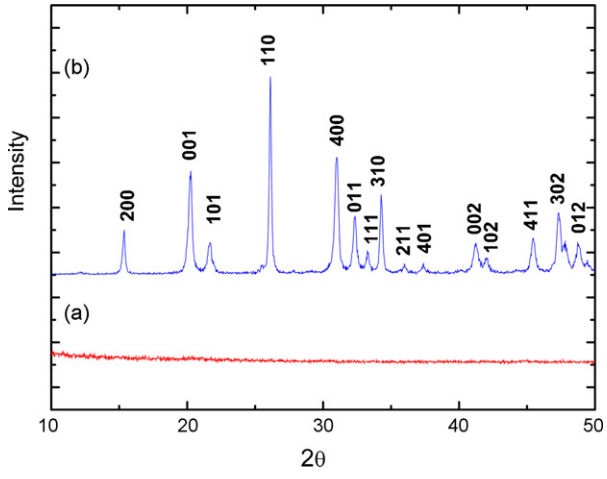

Fig. 6. X-ray diffraction patterns for vanadium pentoxide–carbon cryogels composites at room temperature (a) and after annealing at 400 °C for 2 h (b).

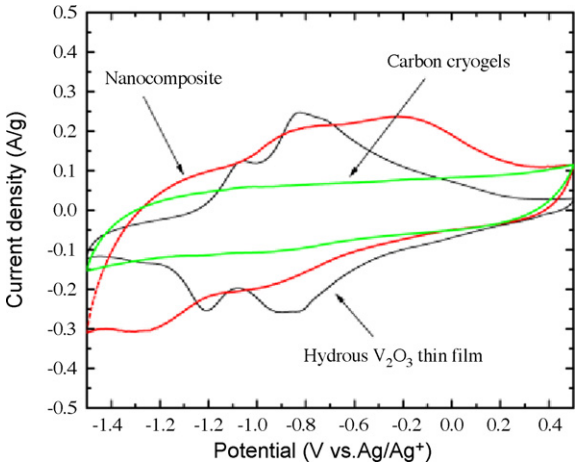

Fig. 7. Cyclic voltammetry curves of hydrous V_2O_5, CCs, and $V_2O_5{\cdot}nH_2O$–CCs in the voltage window between 0.5 and −1.5 V vs. Ag/Ag^+ in 1 M $LiClO_4$ in PC at the scan rate of 1 mV s^{-1}.

potentials caused by different environments of V_2O_5 surrounded with amorphous carbon cryogels for lithium-ions intercalation and deintercalation. Neither cathodic nor anodic peaks for CCs film were observed that demonstrated no lithium-ion electrochemical intercalation into carbon cryogel substrate occurred at this voltage window. Thus the insertion and removal of lithium ions are attributed to hydrous vanadium pentoxide during the charge and discharge process.

Chronopotentiometric measurements were carried out to determine the specific discharge/charge capacities of $V_2O_5{\cdot}nH_2O$–CC nanocomposites and $V_2O_5{\cdot}nH_2O$ films, and the results are shown in Fig. 8. The $V_2O_5{\cdot}nH_2O$ film deposited on platinum substrate possessed an initial specific discharge capacity of 151 mAh g^{-1} at a current density of 100 mA g^{-1} and with a continuous loss in the successive cycles. A capacity of 96 mAh g^{-1} retained after 20 cycles, which only accounted 63.5% of the initial discharge capacity. As to hydrous vanadium pentoxide in the coherent $V_2O_5{\cdot}nH_2O$–CCs nanocomposite, it reached 280 mAh g^{-1} for the initial discharge cycle and the specific discharge capacity remained quite stable for the later cycles. The specific discharge capacity of hydrous vanadium pentoxide in the coherent nanocomposites still possessed 257 mAh g^{-1} after 20 cycles, the capacity fade of which was only 0.5% per cycle.

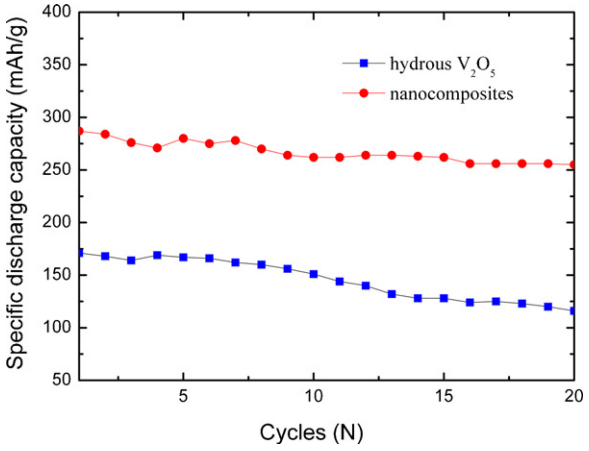

Fig. 8. Plot of specific discharge capacity as a function of cycle numbers for $V_2O_5{\cdot}nH_2O$–CCs and $V_2O_5{\cdot}nH_2O$ on platinum foil and all the mass are based on hydrous vanadium pentoxide.

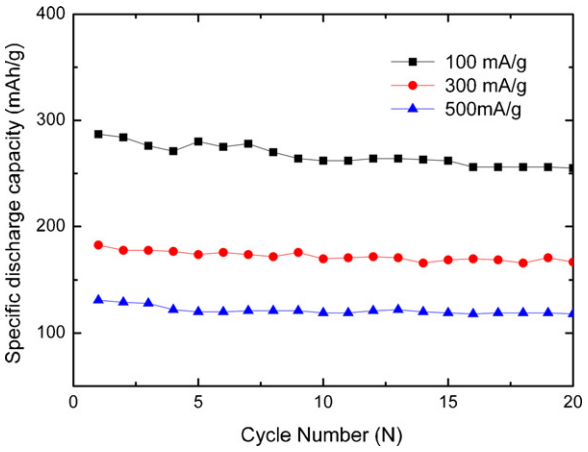

Fig. 9. Discharge capacities as a function of cycle numbers for $V_2O_5{\cdot}nH_2O$–CCs cycled at different current densities (100, 300 and 500 mA g^{-1}) in the voltage window between 0.5 and −1.5 V vs. $Ag/AgNO_3$.

Materials with good electrical conductivity and mass transport are key factors for the success of lithium-ion batteries. The relatively low specific capacity of hydrous $V_2O_5{\cdot}nH_2O$ film could be attributed to the fact that the electrochemical utilization of vanadium pentoxide was limited to the relatively thin surface layer of the oxide film [18]. In contrast, hydrous vanadium pentoxide in nanocomposite may all contribute to lithium intercalation and deintercalation, as the introduction of porous carbon scaffold (carbon cryogel) effectively reduced the diffusion distance for both mass and charge and created large specific surface area for the intercalation and deintercalation reactions. For coherent $V_2O_5{\cdot}nH_2O$–CC nanocomposites with average pore size 6 nm, it had facile pass for lithium ions and, thus, increased the active contact surface area (>400 $m^2\ g^{-1}$) with vanadium pentoxide resulting in much higher capacities. The nanocomposites also demonstrated much improved reversibility of discharge and charge process as shown in Fig. 8a. This may partially be contributed by the porous structure which offered extra space to accommodate the stressed accompanied with lithium ions intercaltion/deintercalation and the coherent carbon network provides extra mechanical support. The discharge capacities of the nanocomposites in the voltage window between 0.5 and −1.5 V at various current densities (100, 300 and 500 mA g^{-1}) as a function of cycle numbers were shown in Fig. 9. Comparing to the earlier hydrous vanadium pentoxide nanotube arrays fabricated by electrodeposition which had a large decay in the first cycles and stabilized at 180 mAh g^{-1} in the later cycles, although with an initial discharge capacity of 300 mAh g^{-1} [33] as-synthesized hydrous vanadium pentoxide and carbon cryogel nanocomposites are much more stable and have better capacitance retention at high current density. It also had similar electrochemical stability to V_2O_5/CTIT nanocomposites at the voltage cutoff of 4–2 V (vs. Li/Li^+), in which carbon tube-in-tube served as an efficient conduction network [19]. It is value nothing that carbon scaffold plays an important role in the nanocomposites.

While it is not known the exact microstructure of the coherent nanocomposites, the particles of hydrous vanadium pentoxide can be smaller than 1 nm in diameter if hydrous vanadium pentoxide conformally coated onto the pore surface of carbon cryogels as the pore diameter reduced from 8 to 6 nm. The absence of XRD peaks before annealing in the as-grown coherent nanocomposite (Fig. 6) might be another indication of very small particles or possible amorphous nature. Small particles with much high surface area (>400 $m^2\ g^{-1}$) would definitely benefit the surface or interface redox reactions during lithium-ion intercalation and deintercalation. The large surface energy and poor crystallinity (or amorphous nature) may allow easy phase transition, leading to a much expanded range of reversible lithium-ion intercalation and deintercalation. Electroactive materials with intentionally designed nanostructures, surface defects and poor crystallinity, for both anode and cathode application have been reported to achieve much enhanced lithium-ion intercalation properties [36–39]. The much improved lithium intercalation properties have been attributed to the extra surface energy or non-equilibrium state of the electroactive materials. Similar explanation might be applicable to this nanocomposites.

4. Conclusions

Potentiodynamic electrochemical deposition has been demonstrated as an effective method to introduce and deposit hydrous vanadium pentoxide into the pores of carbon cryogels to fabricate the coherent CCs–$V_2O_5{\cdot}nH_2O$ nanocomposites. As-fabricated CCs–$V_2O_5{\cdot}nH_2O$ nanocomposites exhibited much high discharge capacity than hydrous vanadium pentoxide film deposited on platinum substrate, with better cyclic stability. By introducing carbon cryogel scaffold, three benefits were assumed: (1) high specific surface area and short diffusion distance to increase the utilization of $V_2O_5{\cdot}nH_2O$ material, (2) good electrical conductive carbon network to facilitate charge transport in the nanocomposites, and (3) void space to accommodate the volume change during the lithium-ion intercalation and deintercalation.

Acknowledgements

This work was supported financially in part by National Science Foundation (DMI-0455994 and DMR-0605159), Air Force Office of Scientific Research (AFOSR-MURI, FA9550-06-1-0326), Pacific Northwest National Laboratories (PNNL), and National Center for Nanomaterials Technology, Korea. A.Q.P. acknowledges the fellowship from the Chinese Scholarship Council and D.W.L. would like to acknowledge the graduate fellowship from the University of Washington Center for Nanotechnology (CNT).

References

[1] J.M. Tarascon, M. Armand, Nature 414 (2001) 359.
[2] J. Hassoun, P. Reale, B. Scrosati, J. Mater. Chem. 17 (2007) 3668.
[3] M. Armand, J.M. Tarascon, Nature 451 (2008) 652.
[4] L. Taberna, S. Mitra, P. Poizot, P. Simon, J.M. Tarascon, Nat. Mater. 5 (2006) 567.
[5] E.A. Ponzio, T.M. Benedetti, R.M. Torresi, Electrochim. Acta 52 (2007) 4419.
[6] Y. Wang, G.Z. Cao, Adv. Mater. 20 (2008) 2251.
[7] Y. Wang, K. Takahashi, K. Lee, G.Z. Cao, Adv. Funct. Mater. 16 (2006) 1133.
[8] J. Livage, Chem. Mater. 3 (1991) 578.
[9] H.K. Park, W.H. Smyrl, M.D. Ward, J. Electrochem. Soc. 142 (1995) 1068.
[10] T. Watanabe, Y. Ikeda, T. Ono, M. Hibino, M. Hosoda, K. Sakai, T. Kudo, Solid State Ionics 151 (2002) 313.
[11] K. Takahashi, Y. Wang, G.Z. Cao, Appl. Phys. Lett. 86 (2005).
[12] K. Takahashi, Y. Wang, G.Z. Cao, J. Phys. Chem. B 109 (2005) 48.
[13] Y. Wang, H.M. Shang, T. Chou, G.Z. Cao, J. Phys. Chem. B 109 (2005) 11361.
[14] E. Baudrin, G. Sudant, D. Larcher, B. Dunn, J.M. Tarascon, Chem. Mater. 18 (2006) 4369.
[15] I. Boyano, M. Bengoechea, I. de Meatza, O. Miguel, I. Cantero, E. Ochoteco, J. Rodriguez, M. Lira-Cantu, P. Gomez-Romero, J. Power Sources 166 (2007) 471.
[16] L. Li, Z.F. Yan, Nanopor. Mater. IV 156 (2005) 523.
[17] A.G.B.C. Satishkumar, M. Nath, C.N.R. Rao, J. Mater. Chem. 10 (2000) 2115.
[18] I.H. Kim, J.H. Kim, B.W. Cho, Y.H. Lee, K.B. Kim, J. Electrochem. Soc. 153 (2006) A989.
[19] X.L. Yong-Sheng Hu, J.-O. Müller, R. Schlögl, J. Maier, D.S. Su, Angew. Chem. Int. Ed. 48 (2009) 210.
[20] R.W. Pekala, J. Mater. Sci. 24 (1989) 3221.
[21] R.W. Pekala, C.T. Alviso, F.M. Kong, S.S. Hulsey, J. Non-Cryst. Solids 145 (1992) 90.
[22] T. Yamamoto, T. Sugimoto, T. Suzuki, S.R. Mukai, H. Tamon, Carbon 40 (2002) 1345.
[23] M.V. Ernest, J.P. Bibler, R.D. Whitley, N.H.L. Wang, Ind. Eng. Chem. Res. 36 (1997) 2775.
[24] E. Frackowiak, F. Beguin, Carbon 39 (2001) 937.

[25] K.S.W. Sing, D.H. Everett, R.A.W. Haul, L. Moscou, R.A. Pierotti, J. Rouquerol, T. Siemieniewska, Pure Appl. Chem. 57 (1985) 603.
[26] K.S.W. Sing, Pure Appl. Chem. 54 (1982) 2201.
[27] B.B. Garcia, A.M. Feaver, Q.F. Zhang, R.D. Champion, G.Z. Cao, T.T. Fister, K.P. Nagle, G.T. Seidler, J. Appl. Phys. 104 (2008).
[28] C. Arbizzani, S. Beninati, M. Lazzari, F. Soavi, M. Mastragostino, J. Power Sources 174 (2007) 648.
[29] S. Sepehri, B.B. Garcia, G.Z. Cao, Eur. J. Inorg. Chem. (2009) 599.
[30] A. Feaver, S. Sepehri, P. Shamberger, A. Stowe, T. Autrey, G.Z. Cao, J. Phys. Chem. B 111 (2007) 7469.
[31] E. Potiron, A.L. La Salle, A. Verbaere, Y. Piffard, D. Guyomard, Electrochim. Acta 45 (1999) 197.
[32] K. Takahashi, S.J. Limmer, Y. Wang, G.Z. Cao, J. Phys. Chem. B 108 (2004) 9795–9800.
[33] Y. Wang, K. Takahashi, H.M. Shang, G.Z. Cao, J. Phys. Chem. B 109 (2005) 3085–3088.
[34] R.J. Al-Muhtaseb, Adv. Mater. 15 (2003) 101.
[35] S. Passerini, J.J. Ressler, D.B. Le, B.B. Owens, W.H. Smyrl, Electrochim. Acta 44 (1999) 2209.
[36] D.W. Liu, B.B. Garcia, Q.F. Zhang, Q. Guo, Y.H. Zhang, S. Sepehri, G.Z. Cao, Adv. Funct. Mater. 19 (2009) 1015–1023.
[37] D.W. Liu, Y.Y. Liu, B.B. Garcia, Q.F. Zhang, A.Q. Pan, Y.H. Jeong, G.Z. Cao, J. Mater. Chem. 19 (2009) 8789–8795.
[38] A.M. Cao, J.S. Hu, H.P. Liang, L.J. Wan, Angew. Chem. Int. Ed. 44 (2005) 4391–4395.
[39] D.H. Wai, D.W. Choi, J. Li, Z.G. Yang, Z.M. Nie, R. Kou, D.H. Hu, C.M. Wang, L.V. Saraf, J.G. Zhang, I.A. Aksay, J. Liu, ACS Nano. 3 (2009) 907–914.